J Appl Electrochem (2016) 46:917–928
DOI 10.1007/s10800-016-0976-7

RESEARCH ARTICLE

Synthesis and electrocatalytic performance of phosphotungstic acid-modified Ag@Pt/MWCNTs catalysts for oxygen reduction reaction

Shuping Yu[1] · Yan Wang[1] · Hong Zhu[1] · Zhongming Wang[1] · Kefei Han[1]

Received: 26 February 2016 / Accepted: 23 May 2016 / Published online: 8 June 2016

Abstract Keggin-structured phosphotungstic acid $H_3PW_{12}O_{40}$ (HPW)-modified Ag@Pt/MWCNTs electrocatalysts were successfully prepared using a chemical impregnation method. Physical characterization by X-ray powder diffraction, high-resolution transmission electron microscopy, scanning electron microscopy, and X-ray photoelectron spectroscopy revealed that the HPW molecules were incorporated into the Ag@Pt/MWCNT structure The diameter of the catalyst used was about 4.0 nm, and electrochemical investigation results indicated that HPW could ameliorate electrocatalytic activity. The catalyst with HPW content of 25 % displayed the best excellent electrocatalytic activity with an electrochemically active area of 83.62 $m^2\ g^{-1}$ and a half-wave potential for the oxygen reduction reaction of 0.851 V, all ascribed to the high utilization of Pt and the protective effect of the HPW layer on the catalyst surface. The synergic effect of the HPW and Ag@Pt enhanced the rate of electron transfer and increased the catalytic efficiency of oxygen reduction reaction, influencing $4e^-$ reduction reactions on Ag@Pt/MWCNTs-HPW catalysts.

Graphical Abstract Phosphotungstic acid-modified Ag@Pt/MWCNTs catalysts were successfully synthesized by the chemical impregnation method. The morphology and catalytic performance of the prepared catalysts were investigated, leading to the understanding of catalytic mechanism of the catalyst in acidic medium, especially, the importance of HPW in the hybrid catalysts. The investigation indicated that the hybrid catalyst showed excellent activity toward oxygen reduction. Schematic diagram for mechanism of ORR on Ag@Pt/MWCNTs-HPW nanostructure.

✉ Shuping Yu
yusp@mail.buct.edu.cn

[1] State Key Laboratory of Chemical Resource Engineering, Faculty of Science, Beijing University of Chemical Technology, Beijing 100029, People's Republic of China

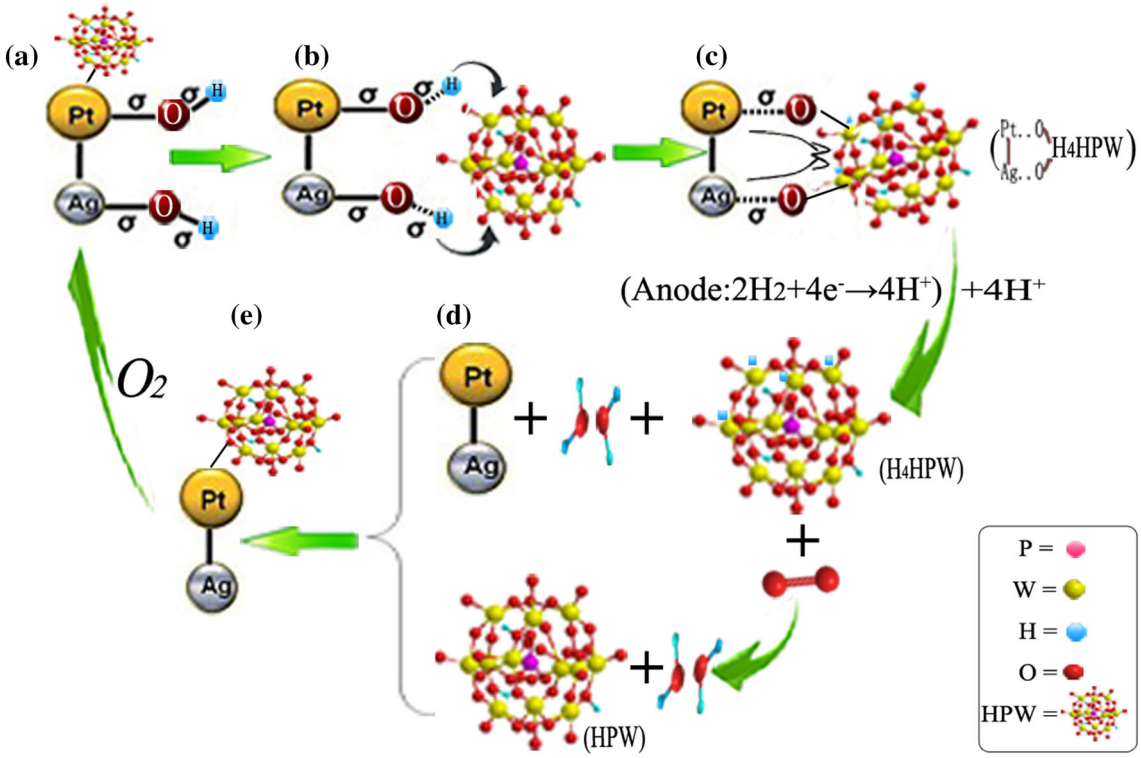

Keywords Heteropolyacid · Keggin-structured HPW · Catalytic mechanism · Electrocatalyst · Oxygen reduction reaction

1 Introduction

Platinum-based catalysts are the most effective catalysts for oxygen reduction reactions (ORRs) in acid media. However, these catalysts are costly and limited in reserve that researchers worldwide have put significant efforts into developing efficient and inexpensive catalysts to overcome such issues in recent years [1–4]. Core–shell catalysts of Pt with other transition metals (Pd, Ni, Cu, Fe, and Ag) can improve the utilization of Pt nanoparticles (NPs) while stimulating catalytic activity [5, 6]. Unfortunately, there are still some drawbacks of the core–shell catalysts, such as poor stability and their potential to poison. Therefore, the activities and stabilities of these Pt-based core–shell catalysts need to be improved. Recently, several studies have been focused on promoting the electrochemical durability of the catalysts [7–11]. For instance, Ying et al. [12] prepared AgPd@Pt NPs by depositing Pt layer on the surface of AgPd alloy NPs, and the specific activity of AgPd@Pt was two times higher than that for Pt/C. Zhao et al. [13] discovered that the nanodiamond@TiN supported Pt NPs by microwave heating polyol method can help to remove the CO or CO-like intermediates and enlarge the Pt/Pt-oxide surface redox couple due to the presence of TiN. Addition of metal oxides (CoO_x, MnO_x, and CeO_x) can also promote the durability of catalysts owing to their corrosion resistance and durability in catalytic reactions [14–16]. For example, the stability of the $Pt/WO_3/C$ catalyst increased 20 % compared with the Pt/C catalyst [17].

Heteropolyacid (HPA), a unique class of inorganic metal−oxygen clusters, is considered to be a promising catalyst in various fields due to its unique physicochemical properties, including non-toxicity, structural variability, ultra-strong Brønsted acidity, low cost, high proton conductivity, and reversible rapid multi-electron transformation under mild conditions [18–20]. Hassan et al. found that HPA as a multi-electron donor accepting conduction band electron can effectively prevent the combination between the hydrogen ions and photoelectrons and improve the photocatalytic activity. Li et al. [21] synthesized photoanodes containing HPA of dye-sensitized solar cells using a solvothermal method, which resulted in an improvement of 49.2 % of the solar electric energy conversion efficiency compared to the performance of photoanodes without HPA. As a novel HPA-based ionic liquid catalyst for *n*-caprylic acid esterification, Han et al. [22] found that there was only 3 % loss in catalytic activity over six consecutive runs, implying excellent durability and recyclability of the catalyst.

Phosphotungstic acid ($H_3PW_{12}O_{40}$, HPW), a member of the Keggin-structured HPA, is outstanding for use in electrocatalytic fields on account of its strong acidity and high proton conductivity [23–26]. Furthermore, Keggin-structured HPW is a large molecule of stable cage structure, in which tetrahedral P atoms and octahedral W atoms are connected via a strong oxygen bridge. The cage structure has some pores that allow oxygen-containing materials to move freely and improve the contact area among reactants [27]. Thus, Keggin-structured HPW has attracted many researchers' attention due to its unique physicochemical characteristics [28–32]. For instance, Xiang et al. prepared a composite membrane combination HPW with Nafion, and the maximum power density of the composite membrane increased by 26 % over the cell performance of pristine Nafion under the same conditions. In addition, due to the good catalytic properties of HPW, the mass activity of the hybrid catalyst combination of HPW with Pt/C was about 3 times higher than that of Pt/C catalyst [33]. The HPW-modified PtRu nanocatalyst can reduce the CO poisoning effect, which may be ascribed to the protective effect of the self-assembled HPW layer on the catalyst surface [34]. Dsoke et al. [35] revealed that the Pt-HPW catalyst proceeded through $4e^-$ reduction of O_2–H_2O, which may be accountable to HPW as a co-catalyst providing a proton-rich environment in the vicinity of the Pt NPs. Some studies have showed that the combination of chitosan (CS) and HPW can greatly enhance the mechanical strength of HPW in solution [36]. Besides, the HPW-CS on carbon can increase the proton conductivity of the carbon support while improving the stability and toxicity tolerance of carbon NPs [37]. Although HPW, as a co-catalyst for ORR, has been the focus of numerous researches, there still exists a certain degree of gaps in meeting the requirements for use in commercialization development.

In this work, inspired by the remarkable works reported and on the basis of our previous studies [38], we immobilized negatively charged HPW on Ag@Pt/MWCNTs NPs attached to positively charged functional groups of CS by electrostatic interaction to obtain HPW-modified Ag@Pt/MWCNTs electrocatalysts. The morphology and catalytic performance of the prepared catalysts were investigated, leading to the understanding of catalytic mechanisms in acidic media and the importance of HPW in hybrid catalysts.

2 Experimental

Multi-walled carbon nanotubes (MWCNTs) were purchased from Shenzhen Nanotech Port Co., Ltd. (Shenzhen, China). Dihydrogen hexachloroplatinate hexahydrate ($H_2PtCl_6{\cdot}6H_2O$,) was purchased from Sinopharm Chemical Reagent Co., Ltd. (Shanghai, China). Keggin-type heteropoly phosphotungstic acid (HPW) was obtained from Sigma-Aldrich (Shanghai, China). CS powder was provided by Haidebei, Ltd., China. Commercial 20 % Pt/C [Johnson–Matthey (JM)] catalyst was purchased from Shanghai Hesen electric Co., Ltd. (Shenzhen, China). Nafion (5 % solution in alcohol) was obtained from DuPont. All other chemicals were purchased from the Beijing Chemical Reagent Store (China) and used without further purification. Double-distilled deionized water was used throughout this study.

2.1 Synthesis of Ag@Pt/MWCNTs electrocatalyst

The core–shell Ag@Pt/MWCNTs (Ag:Pt:C = 10:10:80) electrocatalysts used in this work were prepared using $NaBH_4$ and ethylene glycol as reducing agents and performed as described in our previous work [39].

2.2 Synthesis of Ag@Pt/MWCNTs-HPW electrocatalyst

The as-prepared Ag@Pt/MWCNTs NPs were suspended in a CS-acetic acid solution (2 wt%) using ultrasonication for 30 min with CS acting as the functionalization polyelectrolyte. After stirring for 12 h at room temperature, the solution was filtered and washed with deionized water several times. The CS-functionalized Ag@Pt/MWCNTs NPs were dried at 50°C for 24 h. Then, CS-functionalized Ag@Pt/MWCNTs were sonicated in HPW solution (0.38 mol L^{-1}). After stirring for 3 h, the solution was filtered and washed extensively with deionized water and then dried at 50°C for 24 h. The as-synthesized nanoparticle electrocatalysts are denoted by Ag@Pt/MWCNTs-HPW.

Scheme 1 depiction of the synthesis procedure for the Ag@Pt/MWCNTs-HPW. The Ag@Pt/MWCNTs were prepared as described in a previous study [38]. Then, Ag@Pt/MWCNTs were doped with HPW to obtain Ag@Pt/MWCNTs-HPW electrocatalysts.

2.3 Physical characterizations

The metal phases of the as-prepared electrocatalysts were analyzed with X-ray powder diffraction (XRD, Cu Kα = 1.5406 Å). The high-resolution transmission electron microscopy (HRTEM) was used to observe the particle size and morphology on a JEOL S-520 30 microscope. Scanning electron microscopy (SEM) observations were conducted with a Hitachi S4700 microscope equipped with an electron energy-dispersive X-ray spectrometer (EDX).

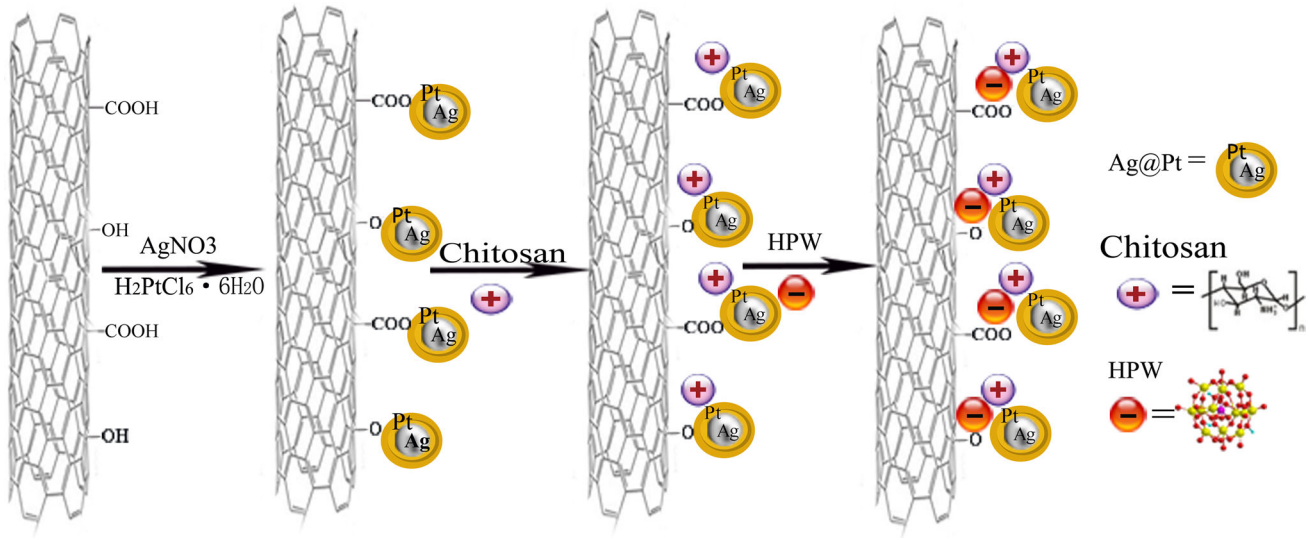

Scheme 1 Schematic diagram for formation of Ag@Pt/MWCNTs-HPW nanostructure

X-ray photoelectron spectroscopy (XPS) analysis was carried out to obtain information on the catalyst surface using a Thermo VGESCALAB250 spectrometer.

2.4 Electrochemical investigation

The electrocatalytic activity of the synthesized catalysts was evaluated by a Zahner Ennium electrochemical workstation equipped with a three-electrode cell installed with platinum wire and Ag/AgCl as the counter electrode and reference electrode. The working electrode was prepared as follows. First, 19.9 mL distilled water and 5.0 mL isopropanol were ultrasonically mixed with 100 μL Nafion solution (5 wt%, Aldrich) for at least 2 h to form a homogeneous solution to be used as dispersant. Then, a catalyst ink was made by mixing 5.0 mg catalyst and 1.0 mL of as-prepared dispersant ultrasonically for at least 30 min. The catalyst ink (10 μL) was perfectly dropped on the center surface of a glassy carbon (GC) electrode (0.196 cm^2) as the working electrode and dried at room temperature. Linear scanning voltammetry (LSV) tests were used to assess the catalytic activity for ORR in O_2-saturated 0.1 mol L^{-1} $HClO_4$ solution. Cyclic voltammetry (CV) and chronoamperometry measurements were conducted in the same solution to study the activity and stability of the electrocatalysts. Electrochemical impedance spectroscopy (EIS) tests were conducted by superimposing a 5 mV ac signal under potentiostatic mode over the frequency range from 0.01 Hz to 100 kHz. All potentials in this study refer to the reversible hydrogen electrode (RHE). All electrochemical measurements were performed at 25 °C.

3 Results and discussion

3.1 Physical characterizations

Figure 1 shows the XRD patterns for the different electrocatalysts recorded in the 2θ range, from 10° to 90°. In Fig. 1, the peak at $2\theta = 26.05°$ is assigned to the characteristic diffraction peak of the carbon support (MWCNTs). For 20 % Pt/MWCNTs, the peaks located at 39.84°, 46.18°, 67.82°, and 81.38° are assigned to the characteristic diffraction peaks of the Pt crystal faces (1 1 1), (2 0 0), (2 2 0), and (3 1 1), respectively. The diffraction peaks of Ag are not obvious in the pattern for Ag@Pt/MWCNTs, indicating that metallic silver formed in the interior of the platinum shell.

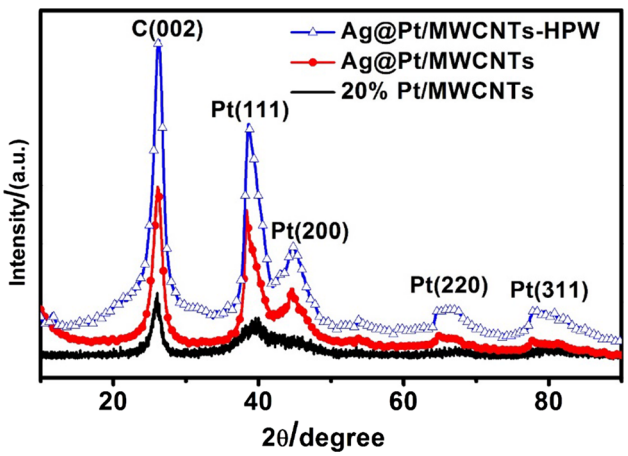

Fig. 1 XRD patterns for different electrocatalysts. Scanning range: 10°–90°, scanning speed: 5° min^{-1}

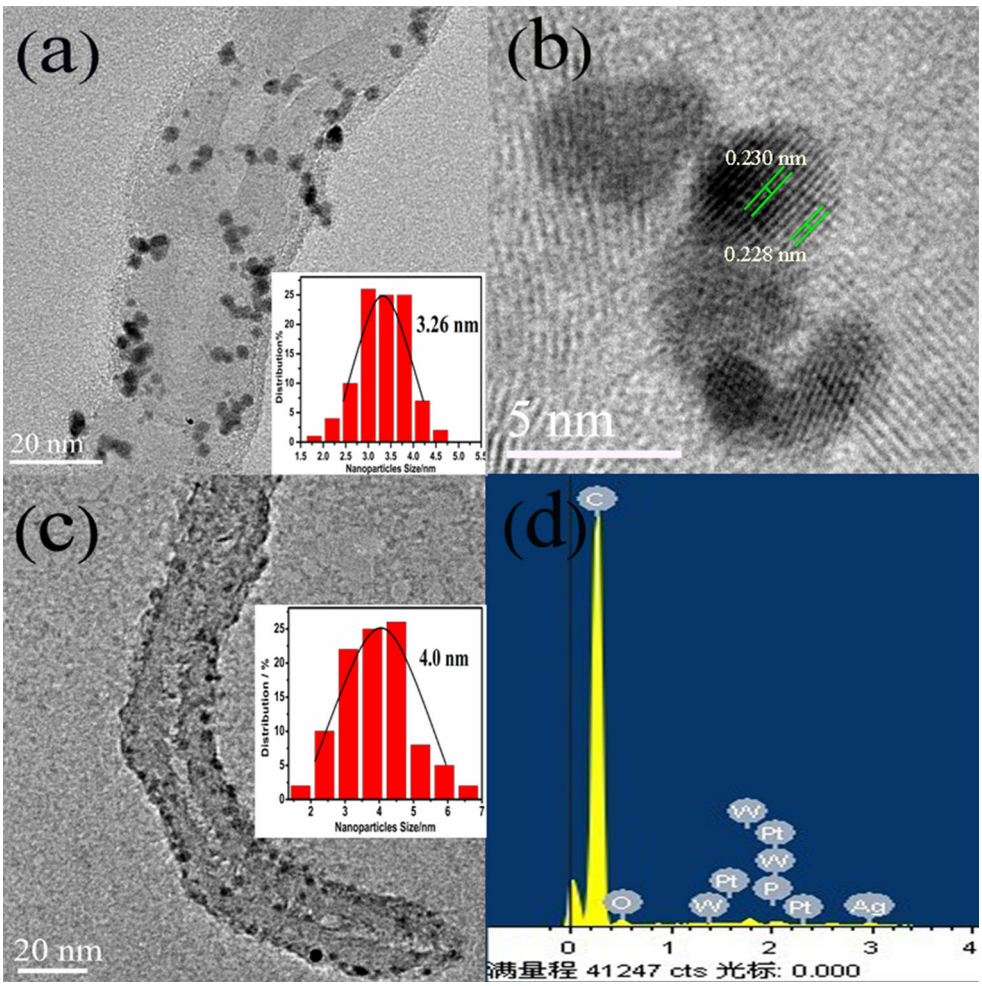

Fig. 2 **a** HRTEM image of Ag@Pt/MWCNTs, **b** HRTEM image of Ag@Pt, **c** TEM image of Ag@Pt/MWCNTs-HPW, **d** EDX analysis of **c**

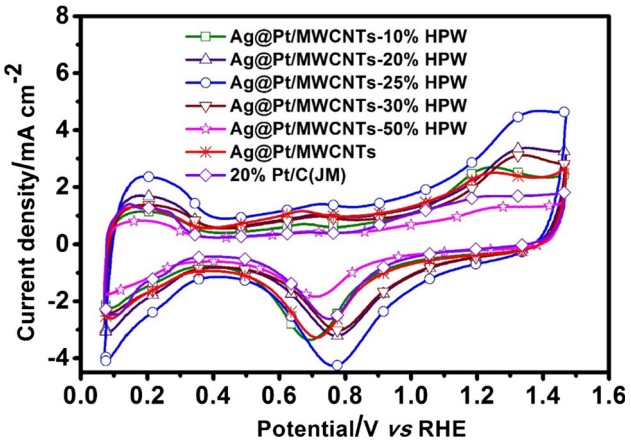

Fig. 3 Cyclic voltammograms of different electrocatalysts. Electrolyte: 0.1 mol L^{-1} $HClO_4$, sweep rate: 50 mV s^{-1}

Compared to 20 % Pt/MWCNTs, the characteristic diffraction peak of the Ag@Pt/MWCNTs electrocatalysts shows a negative shift, where larger Ag atoms replaced Pt atoms in the Pt unit, increasing the size of the platinum unit and the lattice constant. In other words, the inflated Pt lattice sheltered the Ag atoms to form an Ag@Pt system. The size of the Ag@Pt NPs was calculated using the Debye–Scherrer equation (Eq. 1):

$$d = 0.9\lambda/(B\cos\theta), \quad (1)$$

where d is the average size of the NPs (nm), λ is the wavelength of Cu Kα radiation (=1.54056 Å), B is the width of the half peak of the crystal plane, and θ is the measured crystal face diffraction Bragg's angle. The characteristic diffraction peak of the Pt crystal faces in HPW-doped electrocatalysts shows a slight negative shift compared to that in Ag@Pt/MWCNTs. There are no obvious characteristic diffraction peaks for HPW in the XRD pattern of Ag@Pt/MWCNTs-HPW composite, which indicates that HPW exists in the form of a single molecule on the Ag@Pt/MWCNTs catalyst.

Figure 2 shows the TEM and HRTEM images of the different electrocatalysts. From Fig. 2a, the catalyst NPs with an average diameter of about 3.26 nm are uniformly dispersed on the MWCNTs support. The Ag@Pt core–shell

Table 1 Electrochemical results of various catalysts

Catalysts	Metal loading (wt%)		$H_3PW_{12}O_{40}$ (wt%)	EASA/(m^2 g^{-1} Pt)	$E_{1/2}$ (V)	I_m^a (mA m^{-1} Pt)	I_s^b (mA cm^{-2})
	Pt	Ag					
Ag@Pt/MWCNTs-HPW	10	10	0	65.25	0.807	63.37	0.94
	10	10	10	68.01	0.785	69.58	1.16
	10	10	20	70.70	0.796	95.38	1.35
	10	10	25	83.62	0.851	138.62	1.75
	10	10	30	54.83	0.763	78.15	1.47
	10	10	50	49.37	0.752	53.36	1.08
20 % Pt/C (JM)	20	–	–	52.63	0.816	46.26	0.72

[a] Mass activity of platinum around 0.8 V

[b] Specific area activity of platinum around 0.8 V

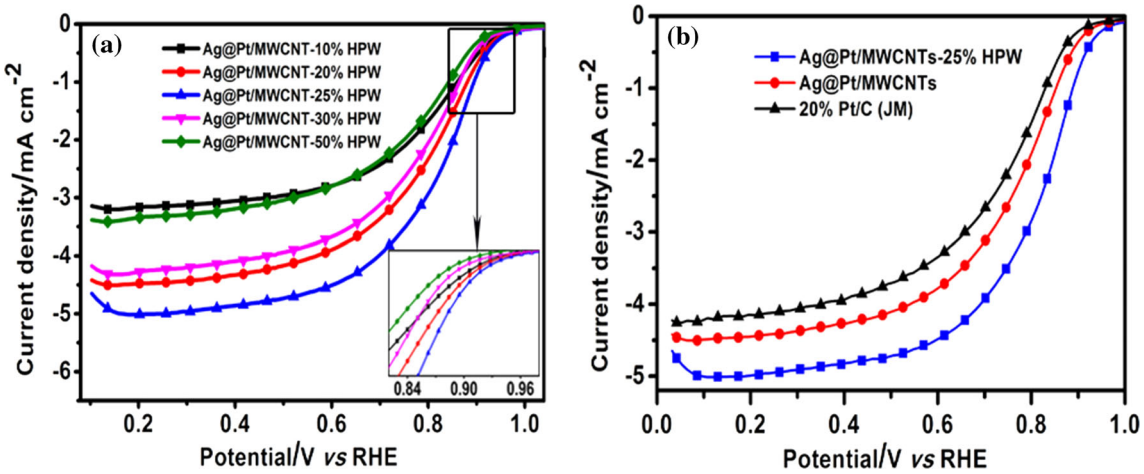

Fig. 4 Polarization curves of different electrocatalysts: **a** Ag@Pt/MWCNTs-HPW with different contents of $H_3PW_{12}O_{40}$; **b** different electrocatalysts. Electrolyte: O_2-saturated 0.1 mol L^{-1} $HClO_4$; sweep rate: 5 mV s^{-1}; rotation speed: 1600 rpm

structure defined from the lattice fringes of the particles is observed in Fig. 2b [38]. After Ag atoms replaced Pt atoms, the platinum lattice expanded, or the platinum lattice atom spacing increased in accordance with the XRD results. The TEM image of Ag@Pt/MWCNT-HPW is displayed in Fig. 2c. After HPW was inserted into Ag@Pt/MWCNT to form a uniform structure, the size of the catalyst NPs increased to 4.0 nm. The surface-specific activity and the electrochemical stability of catalyst improved with the increase in particle size, suggesting that 4.0 nm is the optimum particle size for the maximum ORR mass-specific activity [40]. EDX analysis (Fig. 2d) shows the W and P peaks except Pt and Ag peaks, confirming the existence of HPW on Ag@Pt/MWCNT.

3.2 Electrochemical investigation

The cyclic voltammograms of the different amounts of HPW-modified Ag@Pt/MWCNT catalyst are shown in Fig. 3. The integrated charge of the hydrogen absorption–desorption area of the CV prompted the determination of the corresponding electrochemical active surface areas (EASAs) of the various catalysts [41]:

$$\text{EASA}\left(\text{m}^2\,\text{g}^{-1}\right) = Q_{\text{H}}/(2.1\,[\text{Pt}]), \tag{2}$$

where Q_H is the charge for hydrogen desorption (C m^{-2}), [Pt] is the Pt loading (g m^{-2}), and 2.1 is the charge (C m^{-2}) required to oxidize a monolayer of H_2 on the catalyst. The EASAs of different catalysts were calculated by means of equation (Eq. 2) and listed in Table 1.

The EASA of the electrocatalyst with HPW content of 25 % (83.62 m^2 g^{-1}) is the largest of all the electrocatalysts. The $PW_{12}O_{40}^{3-}$ group establishes a negative electric field over the catalyst surface that protects complex metal anions from being subjected to electrostatic repulsion so as to conserve the active metal species on the catalyst surface [42]. Thus, the incorporation of HPW can improve the electrical conductivity of Ag@Pt/MWCNTs. However, too

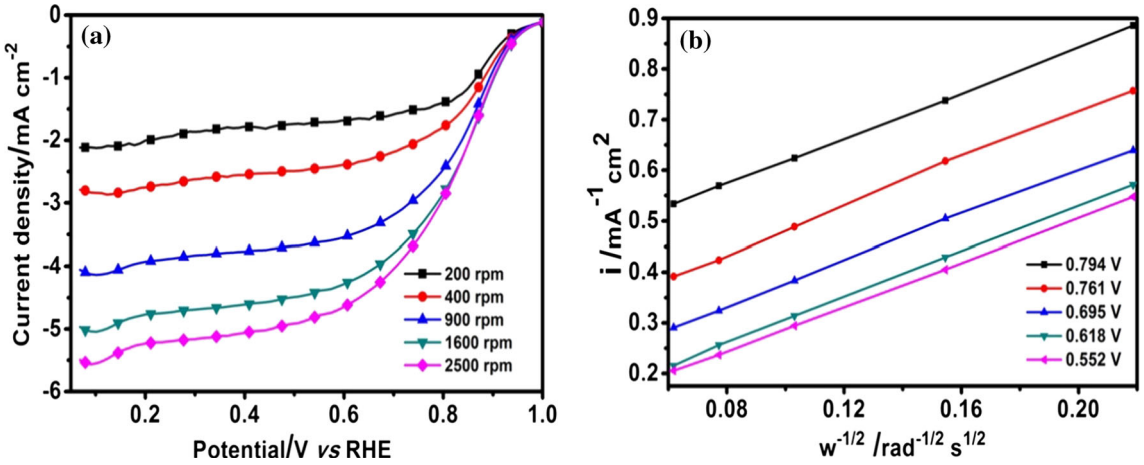

Fig. 5 **a** ORR polarization curves for Ag@Pt/MWCNTs-25 % HPW catalyst in O_2-saturated 0.1 mol L^{-1} $HClO_4$ solution at 25 °C, scan rate of 5 mV s^{-1}, and different rotational speeds: 200, 400, 900, 1600, and 2500 rpm. **b** Corresponding Koutecky–Levich plots at different potentials

Table 2 Number of transferred electrons for various catalysts at various potentials

Catalyst	Potentials (V) versus RHE	Corresponding K–L curves	n^a
Ag@Pt/MWCNTs-25 % HPW	0.552	$y = 2.2417x + 0.0641$, $R^2 = 0.9994$	3.98
	0.618	$y = 2.2538x + 0.08$, $R^2 = 0.9997$	3.96
	0.695	$y = 2.2379x + 0.152$, $R^2 = 0.9994$	3.99
	0.761	$y = 2.265x + 0.2571$, $R^2 = 0.9972$	3.94
	0.794	$y = 2.2619x + 0.3957$, $R^2 = 0.9978$	3.95

[a] Number of transferred electrons

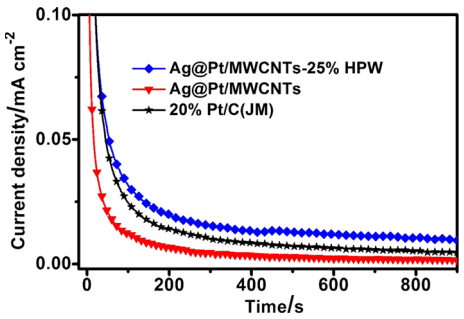

Fig. 6 Chronoamperometry curves for different electrocatalysts: Ag@Pt/MWCNTs, Ag@Pt/MWCNTs-HPW and 20 % Pt/C (JM). Electrolyte: 0.1 mol L^{-1} $HClO_4$; potential: 0.75 V versus NHE; time: 900 s; sweep rate: 50 mV s^{-1}

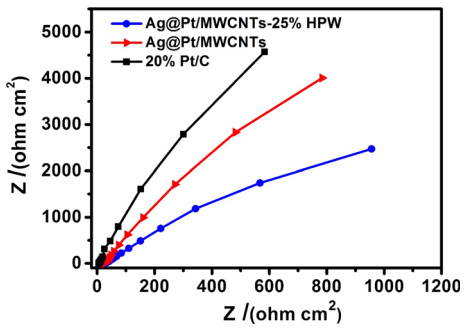

Fig. 7 Nyquist plots of different electrocatalysts: Ag@Pt/MWCNTs, Ag@Pt/MWCNTs-25 % HPW and 20 % Pt/C (JM). Electrolyte: 0.1 mol L^{-1} $HClO_4$; frequency scan: 0.01 Hz–100 kHz; potential: 0.75 V versus NHE

much HPW can obstruct the active site of Pt, increasing the resistance of O_2 from accessing the surface of Pt NPs.

The ORR polarization curves were studied with the catalyst-coated GC electrode, and the current–potential curves are shown in Fig. 4. It was determined that HPW can ameliorate electrocatalytic activity of the catalyst, and the catalyst with HPW content of 25 % displayed the best electrocatalytic activity from Fig. 4a. The half-wave potential ($E_{1/2}$) for the ORR is 0.851 V, which positively shifted 35.0 mV from that of the commercial 20 % Pt/C, revealing that ORR occurs easiest on the surface of the 25 % HPW-modified Ag@Pt/MWCNT catalyst. The mass activity (I_m) and specific area activity (I_s) were evaluated by normalizing the kinetic current (I_k) which was calculated with the Koutecky–Levich equation in consideration of the loading of Pt and ECSAs of the catalysts [43, 44].

The calculated I_m and I_s of Ag@Pt/MWCNT-25 %HPW are about 3.0 and 2.5 times than those of 20 % Pt/C (JM), respectively, as shown in Table 1.

The polarization curves of Ag@Pt/MWCNT-25 % HPW at different electrode rotational speeds shown in Fig. 5a were used to study the ORR kinetic performance. The Koutecky–Levich equation (Eq. 3) was used to calculate the number of electrons transferred per oxygen molecule (n) involved.

$$j^{-1} = j_k^{-1} + \left(0.62nF(D_{O_2})^{2/3}\upsilon^{-1/6}C_{O_2}\omega^{1/2}\right)^{-1}, \quad (3)$$

where j and j_k are the measured current density (mA cm^{-2}) and the kinetic current density (mA cm^{-2}) of the ORR, respectively; n is the overall number of electrons transferred during the ORR; $F(D_{O_2})^{2/3}\upsilon^{-1/6}C_{O_2}$ is the known constant; and ω is the angular velocity of the disk electrode [45]. The curves of j^{-1} and $\omega^{-1/2}$ (K–L curves) at the potentials of 0.794, 0.761, 0.696, 0.618, and 0.552 V are displayed in Fig. 5b.

The n obtained by the Koutecky–Levich equation at each potential is given in Table 2. The results show that the ORR follows a 4e$^-$ pathway from O_2 to H_2O on Ag@Pt/MWCNT-25 % HPW, which indicates that Ag@Pt/MWCNT-25 % HPW has the highest catalytic efficiency [46–48].

Chronoamperometry tests were carried out to study the electrochemical stability of the catalysts at 0.75 V versus NHE in 0.1 mol L^{-1} $HClO_4$ solution [49–51]. As shown in Fig. 6, there is a sharp decrease in the oxidative reaction currents for all electrocatalysts in the beginning. This is because the active sites are covered gradually by the oxygen species OH_{ads} produced during the oxidation reaction process. However, the oxygen-containing species OH_{ads} are continuously generated and removed in the reaction process. When they reach equilibrium, the oxidation currents of all electrocatalysts reach a plateau. Since the large molecular HPW can effectively inhibit the formation of the surface oxygen-containing species OH_{ads}, the Ag@Pt/MWCNTs-25 % HPW catalyst shows the highest current response for continuous catalysis occurring more than 900 s.

EIS measurements were conducted to study the essential actions of the cathodic process [34, 49]. Figure 7 shows the corresponding EIS Nyquist plots of various catalysts at 0.75 V versus NHE in 0.1 mol L^{-1} $HClO_4$ solution. The semicircle diameter at the high frequency used as a measure of catalytic activity is related to the charge transfer resistance of the catalyst for ORR [52, 53]. The diameter of the circular arc for the 25 % HPW-modified Ag@Pt/MWCNTs catalyst is the smallest of all the catalysts in the same frequency range, implying that charge transfer resistance of 25 % HPW-modified Ag@Pt/MWCNTs catalyst for ORR is the lowest. This low resistance helps to accelerate the oxidative removal of oxygen-containing species OH_{ads} adsorbed on the surface of Ag@Pt NPs with HPW and enhances the activity of the 25 % HPW-modified Ag@Pt/MWCNTs catalyst. The negatively charged HPW is combined with positively charged CS onto the Ag@Pt/MWCNTs electrocatalyst via electrostatic attraction, which

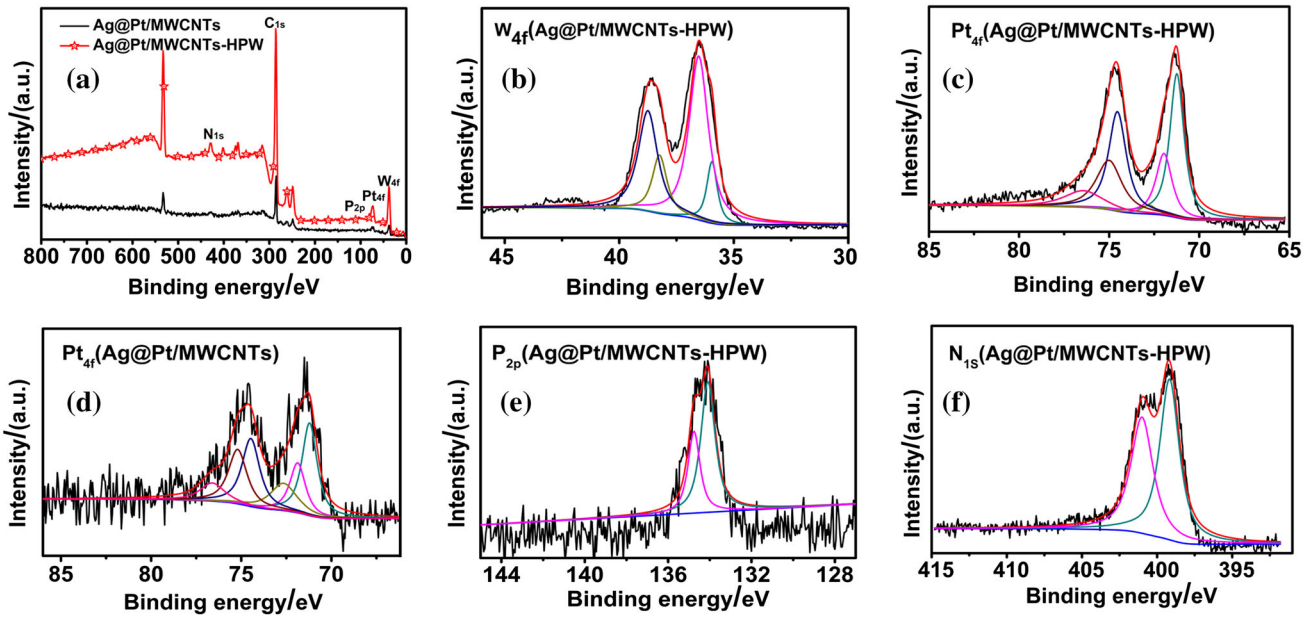

Fig. 8 **a** XPS survey spectrum of Ag@Pt/MWCNTs and Ag@Pt/MWCNTs-HPW catalysts; **b** W_{4f} of Ag@Pt/MWCNTs-HPW; **c** Pt_{4f} of Ag@Pt/MWCNTs-HPW; **d** Pt_{4f} of Ag@Pt/MWCNTs; **e** P_{2p} of Ag@Pt/MWCNTs-HPW; **f** N_{1s} of Ag@Pt/MWCNTs-HPW

Table 3 XPS spectra data of the catalysts

Catalysts	Peak	Binding energy (eV)	Species
Ag@Pt/MWCNTs	Pt_{4f}	71.24, 74.61	Pt
		71.97, 75.45	PtO, $Pt(OH)_2$
		72.63, 77.16	PtO_2
Ag@Pt/MWCNTs-25 %HPW	Pt_{4f}	71.16, 74.53	Pt
		71.94, 75.34	PtO, $Pt(OH)_2$
		72.57, 76.98	PtO_2
	W_{4f}	36.10	WO_2
		38.28	WO_2
		36.68	WO_3
		38.91	WO_3

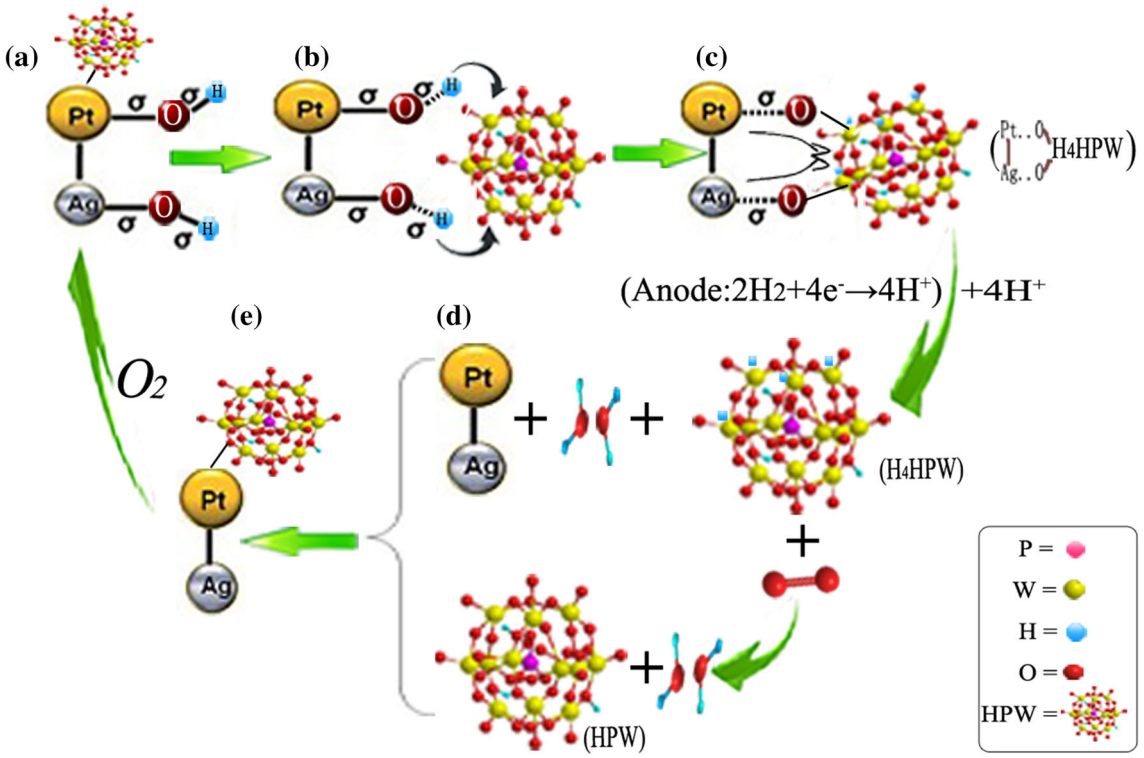

Scheme 2 Schematic diagram for mechanism of ORR on Ag@Pt/MWCNTs-HPW nanostructure

promotes electron transfer and oxygen reaction. The cage structure of HPW provides a tunnel that allows O_2 to adsorb on the surface of the catalyst in a rapid and orderly way, thereby reducing the resistance to the diffusion of oxygen to the surface of the catalyst [54].

XPS measurements were used to distinguish the electronic properties apart from the chemical states and the surface compositions of the catalysts. The XPS spectra obtained for the different catalysts are plotted in Fig. 8. It is obvious that after the incorporation of HPW, W_{4f}, P_{2p}, and N_{1s} peaks appear in the XPS spectrum of Ag@Pt/MWCNTs-25 % HPW (Fig. 8a, b, e, f), which are attributed to HPW and CS. The XPS results reconfirm that HPW molecules have been successfully fixed on the surface of Ag@Pt/MWCNTs. The W_{4f} spectra of Ag@Pt/MWCNTs-25 % HPW are presented in Fig. 8b. The W_{4f} peaks can be divided into two types of doublets with $W_{4f7/2}$ centered at binding energies of 36.5 [W(IV)] and 38.3 eV [W(VI)], and the curve-fitting data are listed in Table 3. In Ag@Pt/MWCNTs-25 % HPW, tungsten exhibits mixed chemical states with surface contents of W(IV) and W(VI).

The Pt_{4f} spectra of Ag@Pt/MWCNTs-25 % HPW and Ag@Pt/MWCNTs are presented in Fig. 8c, d, respectively. As compared with Ag@Pt/MWCNTs, the binding energy

of Pt_{4f} shifts negatively after incorporation of HPW. The existence of HPW in Ag@Pt/MWCNTs leads to a downward shift in the d-band center of Pt and, therefore, HPW can weaken the adsorption of the oxygen-containing species OH_{ads} on the surface of the Pt NPs and increase the catalytic activity of Ag@Pt/MWCNTs-HPW electrocatalyst [37].

According to the above results, the mechanism of ORR on Ag@Pt/MWCNTs-HPW is summarized in Scheme 2. As described in our previous study [39], O_2 easily accepts e^- and H^+ to form OH_{ads} and undergoes double adsorption on the surface of Pt (Pt-OH, Scheme 2a). The double adsorption is the rate-determining step of ORR, but the surface oxide formation ($Pt + H_2O \rightarrow$ Pt-OH $+ H^+ + e^-$) hinders further adsorption of O_2. The Ag@Pt structure can weaken the adsorption of the OH_{ads} on the surface of the catalyst. However, the catalyst doped with HPW is more able to reduce the adsorption energy of the Pt-OH (Scheme 2b). On one hand, W–O–Pt bonds can form between W and the oxygenated Pt species because the d orbitals of W ($5d^46s^2$) have a stronger ability to accept electrons than that of Pt ($5d^96s^1$), and electrons are transferred to HPW from the oxygenated Pt species (Scheme 2c). Pt, after losing OH_{ads}, can adsorb O_2 continuously, resulting in acceleration of the ORR and improvement of the activity of the catalyst. Contrarily, HPW accepts protons and electrons to form H_4HPW (HPW $+ 4H^+ + 4e^- \rightarrow H_4$HPW) (Scheme 2c) [55], and then O_2 chemisorbed onto the H_4HPW surface is reduced to H_2O (H_4HPW $+ O_2 \rightarrow$ HPW $+ H_2O$) (Scheme 2d) [56]. The removal of the oxygen-containing OH_{ads} from the surface of the Pt accelerates the double adsorption of O_2 and increases the electron transfer coefficient of the ORR rate-determining step, leading to the enhancement of the activity and stability of the catalyst for ORR [57]. Therefore, the synergic effect of the HPW and the Ag@Pt augments the rate of electron transfer and increases the catalytic efficiency for ORR.

4 Conclusion

In this study, an HPW-modified Ag@Pt/MWCNTs electrocatalyst was successfully prepared using the chemical impregnation method. Physical characterization indicated that the HPW molecules inserted into Ag@Pt/MWCNT formed a uniform structure, and the diameter of the catalyst was about 4.0 nm. Electrochemical investigation results indicated that Ag@Pt/MWCNTs catalyst incorporation with 25 % HPW displayed excellent electrocatalytic activities, which is attributed to the high utilization of Pt and the protective effect of the HPW layer on the catalyst surface. The synergic effect of the HPW and Ag@Pt enhanced the rate of electron transfer and increased the catalytic efficiency of oxygen reduction reaction, influencing $4e^-$ reduction reactions on Ag@Pt/MWCNTs-HPW catalysts. Thus, Ag@Pt/MWCNTs-HPW can be used as a promising cathode catalyst for ORR.

Acknowledgments The authors gratefully acknowledge the financial supports from the National Natural Science Foundation of China (Nos. 21176022, 21176023, 21276021, and 21376022), the International S&T Cooperation Program of China (No. 2013DFA51860), the National High Technology Research and Development Program of China (No. 2011AA11A273), the Program for Changjiang Scholars and Innovative Research Team in University (IRT1205), and the Fundamental Research Funds for the Central Universities (YS1406).

References

1. Zhu J, Wang P-C, Lu M (2015) Study on the one-pot oxidative esterification of glycerol with MOF supported polyoxometalates as catalyst. Catal Sci Technol 5(6):3383–3393. doi:10.1039/c5cy00102a
2. Park S-A, Lim H, Kim Y-T (2015) Enhanced oxygen reduction reaction activity due to electronic effects between Ag and Mn_3O_4 in alkaline media. ACS Catal 5(7):3995–4002. doi:10.1021/acscatal.5b00495
3. Liu M, Li J (2015) Heating treated carbon nanotubes as highly active electrocatalysts for oxygen reduction reaction. Electrochim Acta 154:177–183. doi:10.1016/j.electacta.2014.12.039
4. Fiala R, Vaclavu M, Vorokhta M, Khalakhan I, Lavkova J, Potin V, Matolinova I, Matolin V (2015) Proton exchange membrane fuel cell made of magnetron sputtered Pt–CeOx and Pt–Co thin film catalysts. J Power Sources 273:105–109. doi:10.1016/j.jpowsour.2014.08.093
5. Rashid M, Jun T-S, Jung Y, Kim YS (2015) Bimetallic core–shell Ag@Pt nanoparticle-decorated MWNT electrodes for amperometric H2 sensors and direct methanol fuel cells. Sens Actuators B Chem 208:7–13. doi:10.1016/j.snb.2014.11.005
6. Zhang G, Shao Z-G, Lu W, Xie F, Xiao H, Qin X, Yi B (2013) Core–shell Pt modified Pd/C as an active and durable electrocatalyst for the oxygen reduction reaction in PEMFCs. Appl Catal B 132–133:183–194. doi:10.1016/j.apcatb.2012.11.029
7. Zhao R, Liu Y, Liu C, Xu G, Chen Y, Tang Y, Lu T (2014) Pd@Pt core–shell tetrapods as highly active and stable electrocatalysts for the oxygen reduction reaction. J Mater Chem A 2(48):20855–20860. doi:10.1039/c4ta04917a
8. Zhong X, Yu H, Wang X, Liu L, Jiang Y, Wang L, Zhuang G, Chu Y, Li X, Wang JG (2014) Pt@Au nanorods uniformly decorated on pyridyne cycloaddition graphene as a highly effective electrocatalyst for oxygen reduction. ACS Appl Mater Interface 6(16):13448–13454. doi:10.1021/am5020452
9. Goto S, Hosoi S, Arai R, Tanaka S, Umeda M, Yoshimoto M, Kudo Y (2014) Particle-size-and Ru-core-induced surface electronic states of Ru-core/Pt-shell electrocatalyst nanoparticles. J Phys Chem C 118(5):2634–2640. doi:10.1021/jp411871y
10. Gómez-Marín AM, Feliu JM (2015) Oxygen reduction on nanostructured platinum surfaces in acidic media: promoting effect of surface steps and ideal response of Pt(111). Catal Today 244:172–176. doi:10.1016/j.cattod.2014.05.009
11. Duan H, Hao Q, Xu C (2014) Nanoporous PtFe alloys as highly active and durable electrocatalysts for oxygen reduction reaction. J Power Sources 269:589–596. doi:10.1016/j.jpowsour.2014.07.026

12. Jinhua Yang JY, Ying JackieY (2012) Morphology and lateral strain control of Pt nanoparticles via core–shell construction using alloy AgPd core toward oxygen reduction reaction. Am Chem Soc 6(11):9373–9382. doi:10.1021/nn303298s
13. Zhao Y, Wang Y, Dong L, Zhang Y, Huang J, Zang J, Lu J, Xu X (2014) Core-shell structural nanodiamond@TiN supported Pt nanoparticles as a highly efficient and stable electrocatalyst for direct methanol fuel cells. Electrochim Acta 148:8–14. doi:10.1016/j.electacta.2014.10.024
14. Ma L, Zhao X, Si F, Liu C, Liao J, Liang L, Xing W (2010) A comparative study of Pt/C and Pt–MoOx/C catalysts with various compositions for methanol electro-oxidation. Electrochim Acta 55(28):9105–9112. doi:10.1016/j.electacta.2010.08.034
15. Tiido K, Alexeyeva N, Couillard M, Bock C, MacDougall BR, Tammeveski K (2013) Graphene–TiO_2 composite supported Pt electrocatalyst for oxygen reduction reaction. Electrochim Acta 107:509–517. doi:10.1016/j.electacta.2013.05.155
16. Yu S, Liu Q, Yang W, Han K, Wang Z, Zhu H (2013) Graphene–CeO_2 hybrid support for Pt nanoparticles as potential electrocatalyst for direct methanol fuel cells. Electrochim Acta 94:245–251. doi:10.1016/j.electacta.2013.01.149
17. Dou M, Hou M, Li Z, Wang F, Liang D, Shao Z, Yi B (2015) Pt/WO_3/C nanocomposite with parallel WO_3 nanorods as cathode catalyst for proton exchange membrane fuel cells. J Energy Chem 24(1):39–44. doi:10.1016/s2095-4956(15)60282-0
18. Chojak M, Kolary-Zurowska A, Wlodarczyk R, Miecznikowski K, Karnicka K, Palys B, Marassi R, Kulesza PJ (2007) Modification of Pt nanoparticles with polyoxometallate monolayers: competition between activation and blocking of reactive sites for the electrocatalytic oxygen reduction. Electrochim Acta 52(18):5574–5581. doi:10.1016/j.electacta.2007.01.063
19. Zeng J, Shen PK, Lu S, Xiang Y, Li L, De Marco R, Jiang SP (2012) Correlation between proton conductivity, thermal stability and structural symmetries in novel HPW-meso-silica nanocomposite membranes and their performance in direct methanol fuel cells. J Membr Sci 397–398:92–101. doi:10.1016/j.memsci.2012.01.018
20. Walsh JJ, Bond AM, Forster RJ, Keyes TE (2016) Hybrid polyoxometalate materials for photo(electro-) chemical applications. Coord Chem Rev 306:217–234. doi:10.1016/j.ccr.2015.06.016
21. Li J, Sang X, Chen W, Qin C, Wang S, Su Z, Wang E (2013) The application of ZnO nanoparticles containing polyoxometalates in dye-sensitized solar cells. Eur J Inorg Chem 10–11:1951–1959. doi:10.1002/ejic.201201120
22. Han X, Chen K, Du H, Tang X-J, Hung C-T, Lin K-C, Liu S-B (2015) Novel Keggin-type $H_4PVMo_{11}O_{40}$-based ionic liquid catalysts for n-caprylic acid esterification. J Taiwan Inst Chem E. doi:10.1016/j.jtice.2015.07.005
23. Kim WB, Voitl T, Rodriguez-Rivera GJ, Dumesic JA (2004) Powering fuel cells with CO via aqueous polyoxometalates and gold catalysts. Science 305(5688):1280–1283. doi:10.1126/science.1100860
24. Fan J, Zhu H, Li R, Chen N, Han K (2014) Layered double hydroxide–polyphosphazene-based ionomer hybrid membranes with electric field-aligned domains for hydroxide transport. J Mater Chem A 2(22):8376. doi:10.1039/c4ta00686k
25. Han DM, Guo ZP, Zhao ZW, Zeng R, Meng YZ, Shu D, Liu HK (2008) Polyoxometallate-stabilized Pt–Ru catalysts on multi-walled carbon nanotubes: influence of preparation conditions on the performance of direct methanol fuel cells. J Power Sources 184(2):361–369. doi:10.1016/j.jpowsour.2008.03.051
26. Seo MH, Choi SM, Kim HJ, Kim JH, Cho BK, Kim WB (2008) A polyoxometalate-deposited Pt/CNT electrocatalyst via chemical synthesis for methanol electrooxidation. J Power Sources 179(1):81–86. doi:10.1016/j.jpowsour.2007.12.107
27. Sun Z, Wang S, Wang X, Jiang Z (2016) Lysine functional heteropolyacid nanospheres as bifunctional acid–base catalysts for cascade conversion of glucose–levulinic acid. Fuel 164:262–266. doi:10.1016/j.fuel.2015.10.014
28. Lu J, Tang H, Lu S, Wu H, Jiang SP (2011) A novel inorganic proton exchange membrane based on self-assembled HPW-meso-silica for direct methanol fuel cells. J Mater Chem 21(18):6668. doi:10.1039/c0jm03695a
29. Fan L, Chen H, Xiao D, Wang E (2013) Synthesis, structure, and characterization of a new metal–organic framework containing meso-helices. Z Anorg Allg Chem 639(3–4):558–562. doi:10.1002/zaac.201200474
30. Shi Z, Zhou Y, Zhang L, Mu C, Ren H, Hassan Du, Yang D, Asif HM (2014) New supramolecular compounds based on porphyrin and polyoxometalate: synthesis, characterization and nonlinear optical and optical limiting properties. RSC Adv 4(91):50277–50284. doi:10.1039/c4ra09384d
31. Zhang L, Zhang R, Zhou Y, Qin L (2014) Assembling polyoxometalate microcrystals into thin films with preferential [110]-orientation. Mater Lett 124:36–38. doi:10.1016/j.matlet.2014.03.015
32. Zhen H, Li X, Zhang L, Lei H, Yu C, Zhou Y, Hassan Su, Qin L, Asif HM (2015) Polyoxometalate-based layered nano-tubular arrays: facile fabrication and superior performance for catalysis. RSC Adv 5(31):24550–24557. doi:10.1039/c5ra01247c
33. Li S, Yu X, Zhang G, Ma Y, Yao J, de Oliveira P (2011) Green synthesis of a Pt nanoparticle/polyoxometalate/carbon nanotube tri-component hybrid and its activity in the electrocatalysis of methanol oxidation. Carbon 49(6):1906–1911. doi:10.1016/j.carbon.2011.01.015
34. Chen W, Wei X, Zhang Y (2014) A comparative study of tungsten-modified PtRu electrocatalysts for methanol oxidation. Int J Hydrogen Energy 39(13):6995–7003. doi:10.1016/j.ijhydene.2014.02.147
35. Dsoke S, Kolary-Zurowska A, Zurowski A, Mignini P, Kulesza PJ, Marassi R (2011) Rotating disk electrode study of $Cs_{2.5}H_{0.5}PW_{12}O_{40}$ as mesoporous support for Pt nanoparticles for PEM fuel cells electrodes. J Power Sources 196(24):10591–10600. doi:10.1016/j.jpowsour.2011.09.010
36. Lu S, Wu C, Liang D, Tan Q, Xiang Y (2014) Layer-by-layer self-assembly of Nafion–[CS–PWA] composite membranes with suppressed vanadium ion crossover for vanadium redox flow battery applications. RSC Adv 4(47):24831–24837. doi:10.1039/c4ra01775g
37. Wang D, Lu S, Xiang Y, Jiang SP (2011) Self-assembly of HPW on Pt/C nanoparticles with enhanced electrocatalysis activity for fuel cell applications. Appl Catal B Environ 103(3–4):311–317. doi:10.1016/j.apcatb.2011.01.037
38. Yu S, Lou Q, Han K, Wang Z, Zhu H (2012) Synthesis and electrocatalytic performance of MWCNT-supported Ag@Pt core–shell nanoparticles for ORR. Int J Hydrogen Energy 37(18):13365–13370. doi:10.1016/j.ijhydene.2012.06.109
39. Yu S, Liu R, Yang W, Han K, Wang Z, Zhu H (2014) Synthesis and electrocatalytic performance of MnO_2-promoted Ag@Pt/MWCNT electrocatalysts for oxygen reduction reaction. J Mater Chem A 2(15):5371. doi:10.1039/c3ta14564f
40. Xu Z, Zhang H, Zhong H, Lu Q, Wang Y, Su D (2012) Effect of particle size on the activity and durability of the Pt/C electrocatalyst for proton exchange membrane fuel cells. Appl Catal B Environ 111–112:264–270. doi:10.1016/j.apcatb.2011.10.007
41. Wang R, Li H, Feng H, Wang H, Lei Z (2010) Preparation of carbon-supported core@shell PdCu@PtRu nanoparticles for methanol oxidation. J Power Sources 195(4):1099–1102. doi:10.1016/j.jpowsour.2009.08.055
42. Patel PP, Datta MK, Velikokhatnyi OI, Jampani P, Hong D, Poston JA, Manivannan A, Kumta PN (2015) Nanostructured

robust cobalt metal alloy based anode electro-catalysts exhibiting remarkably high performance and durability for proton exchange membrane fuel cells. J Mater Chem A 3(26):14015–14032. doi:10.1039/c5ta01362c
43. Pech-Pech IE, Gervasio DF, Godínez-Garcia A, Solorza-Feria O, Pérez-Robles JF (2015) Nanoparticles of Ag with a Pt and Pd rich surface supported on carbon as a new catalyst for the oxygen electroreduction reaction (ORR) in acid electrolytes: part 1. J Power Sources 276:365–373. doi:10.1016/j.jpowsour.2014.09.112
44. Luo M, Wei L, Wang F, Han K, Zhu H (2014) Gram-level synthesis of core–shell structured catalysts for the oxygen reduction reaction in proton exchange membrane fuel cells. J Power Sources 270:34–41. doi:10.1016/j.jpowsour.2014.07.102
45. Yan Z, Zhang M, Xie J, Zhu J, Shen PK (2015) A bimetallic carbide Fe2MoC promoted Pd electrocatalyst with performance superior to Pt/C towards the oxygen reduction reaction in acidic media. Appl Catal B Environ 165:636–641. doi:10.1016/j.apcatb.2014.10.070
46. Nie Y, Li L, Wei Z (2015) Recent advancements in Pt and Pt-free catalysts for oxygen reduction reaction. Chem Soc Rev 44(8):2168–2201. doi:10.1039/c4cs00484a
47. Chung YH, Kim SJ, Chung DY, Park HY, Sung YE, Yoo SJ, Jang JH (2015) Third-body effects of native surfactants on Pt nanoparticle electrocatalysts in proton exchange fuel cells. Chem Commun 51(14):2968–2971. doi:10.1039/c4cc09019e
48. Wang Q, Cui X, Guan W, Zhang L, Fan X, Shi Z, Zheng W (2014) Shape-dependent catalytic activity of oxygen reduction reaction (ORR) on silver nanodecahedra and nanocubes. J Power Sources 269:152–157. doi:10.1016/j.jpowsour.2014.06.160
49. Armenta-González AJ, Carrera-Cerritos R, Guerra-Balcázar M, Arriaga LG, Ledesma-García J (2014) Comparative study of carbon-supported Pd and PdAg catalysts synthesised by the polyol process and reverse micelles methods. J Appl Electrochem 45(1):33–41. doi:10.1007/s10800-014-0776-x
50. Du C, Chen M, Wang W, Tan Q, Xiong K, Yin G (2013) Platinum-based intermetallic nanotubes with a core–shell structure as highly active and durable catalysts for fuel cell applications. J Power Sources 240:630–635. doi:10.1016/j.jpowsour.2013.05.023
51. Liao H, Zhu J, Hou Y (2014) Synthesis and electrocatalytic properties of PtBi nanoplatelets and PdBi nanowires. Nanoscale 6(2):1049–1055. doi:10.1039/c3nr05590f
52. Seifitokaldani A, Savadogo O, Perrier M (2015) Stability and catalytic activity of titanium oxy-nitride catalyst prepared by in situ urea-based sol–gel method for the oxygen reduction reaction (ORR) in acid medium. Int J Hydrogen Energy 40(33):10427–10438. doi:10.1016/j.ijhydene.2015.06.002
53. Jin X, He B, Miao J, Yuan J, Zhang Q, Niu L (2012) Stabilization and dispersion of PtRu and Pt nanoparticles on multiwalled carbon nanotubes using phosphomolybdic acid, and the use of the resulting materials in a direct methanol fuel cell. Carbon 50(8):3083–3091. doi:10.1016/j.carbon.2012.03.004
54. El Ali B, El-Ghanam AM, M Fettouhi M (2001) H3 + nPMo12 − nVnO40-catalyzed selective oxidation of benzoins to benzils or aldehydes and esters by dioxygen. J Mol Catal A 165:283–290
55. Wlodarczyk R, Chojak M, Miecznikowski K, Kolary A, Kulesza PJ, Marassi R (2006) Electroreduction of oxygen at polyoxometallate-modified glassy carbon-supported Pt nanoparticles. J Power Sources 159(2):802–809. doi:10.1016/j.jpowsour.2005.11.061
56. Stanis RJ, Kuo M-C, Rickett AJ, Turner JA, Herring AM (2008) Investigation into the activity of heteropolyacids towards the oxygen reduction reaction on PEMFC cathodes. Electrochim Acta 53(28):8277–8286. doi:10.1016/j.electacta.2008.06.052
57. Tymoczko J, Calle-Vallejo F, Colic V, Koper MTM, Schuhmann W, Bandarenka AS (2014) Oxygen reduction at a Cu-modified Pt(111) model electrocatalyst in contact with Nafion polymer. ACS Catal 4(10):3772–3778. doi:10.1021/cs501037y